Distribution functions for reversibly self-assembling spherocylinders

Eric M. Kramer* and Judith Herzfeld
Department of Chemistry, Brandeis University, Waltham, Massachusetts 02454-9110
(Received 3 April 1998)

We consider an equilibrium solution of hard spheres undergoing reversible self-assembly into spherocylinders. Our main interest is the distribution of cylinder orientations and lengths in the nematic phase. Over a limited range of concentrations, we find accurate numerical results for the distribution using an iterative equation. Based on trends in this regime, a trial distribution function is introduced that allows an efficient calculation of accurate thermodynamic data over the entire concentration range. In agreement with previous authors, we find a first-order transition from a dilute, weakly polymerized, isotropic phase to a concentrated, highly polymerized, nematic phase. [S1063-651X(98)09911-5]

PACS number(s): 61.30.−v, 64.70.Md, 87.15.−v

I. INTRODUCTION

The theory of self-assembling filaments has applications to both biology and physics [1]. In ordinary cells, about 10% of the protein is capable of reversible self-assembly into filaments. These proteins, primarily responsible for the cytoskeleton, include actin and tubulin. There are also examples from disease pathology in which normally globular proteins assemble into filaments. The best known disease of this sort is sickle-cell anemia [2]. An improved understanding of these cellular systems has been sought through *in vitro* experiments on solutions containing the minimum required for polymerization (see, e.g., [3–5]). Of equal interest are solutions of smaller amphiphilic molecules [6]. A variety of polyaromatic molecules are known to spontaneously stack to form cylindrical aggregates and many surfactant systems form cylindrical micelles. Both systems exhibit liquid crystal phase behavior, typically an isotropic-nematic or isotropic-hexagonal phase transition.

An important feature common to systems of asymmetrically shaped particles is the presence of a first-order phase transition from an isotropic phase at low concentrations to a nematic phase at high concentrations. The theory of the isotropic-nematic (I-N) phase transition in simple lyotropic liquid crystals is well established. In a seminal paper, Onsager considered a monodisperse solution of hard, rigid spherocylinders and rigorously demonstrated the existence of an I-N transition in the long rod limit [7]. The theory has subsequently been refined to include the effects of finite length and polydispersity [8], electrostatic repulsion [9], and flexibility [10] (see Refs. [11] and [12] for reviews).

The extension of these theories to a polydisperse mixture of rigid rods formed by reversible assembly is less advanced. In this case one needs to find the equilibrium distribution of rods as a function of both orientation and length. Although the law of mass action can be used to reduce the distribution to a single function of azimuthal angle, the solution for that function is qualitatively more difficult than in the monodisperse case. Most previous research has proceeded by making a variety of *ad hoc* assumptions. These include the use of a Gaussian orientation distribution [13], the restriction of rod orientations to three mutually orthogonal axes [14,15], or the assumption that the rods are monodisperse [16,17].

To our knowledge, there have only been two previous attempts to derive an accurate and self-consistent length and orientation distribution. van der Schoot and Cates [18] expanded the distribution in Legendre polynomials and solved for the coefficients in the vicinity of the isotropic-nematic bifurcation point. This approach was necessarily limited to very weakly ordered phases (order parameter less than 0.03). Hentschke and Herzfeld [19] solved the nonlinear integral equation for the distribution using a numerical iterative scheme, but we will show that they lacked sufficient angular resolution to find accurate results in the nematic phase.

The goal of this paper is to obtain the accurate equilibrium distribution function, free energy, and associated thermodynamic results for a solution of reversibly self-assembling spherocylinders. We employ a phenomenological description of rod assembly and a scaled particle treatment of excluded volume effects [8]. (Use of Onsager's second virial approximation instead of scaled particle theory gives less accurate results, but does not change our qualitative conclusions.) We find that the nematic orientation distribution exhibits approximately *linear* behavior at small angles, in contrast to previous assumptions. We also provide accurate results for the free energy of the nematic phase over the entire concentration range. In agreement with previous authors, we find a transition between an isotropic phase of short rods at low volume fractions and a nematic phase of long rods at high volume fractions. The only thermodynamically stable nematic phase is fully polymerized and has volume fraction $v=1$, corresponding to the length ''explosion'' reported by Odijk [17].

The paper is organized as follows. In Sec. II we present the free energy of a polydisperse mixture of hard spherocylinders formed by the reversible, isodesmic, self-assembly of spheres. In Sec. III we derive an integral equation for the rod distribution that minimizes the free energy. The integral equation is solved iteratively, but convergence is very slow over most of the nematic phase. In Sec. IV we present a four-parameter trial function for the rod distribution that captures the essential features of the iterative solution and al-

*Present address: Physics Department, Williams College, Williamstown, MA 01267.

lows us to minimize the free energy much more rapidly. In Sec. V we discuss some qualitative features of the solution at high volume fractions and derive accurate closed expressions for the free energy and mean polymerization. In Sec. VI we calculate the pressure and other thermodynamic quantities for the free energies of Secs. III–V. In Sec. VII we compare our results to an approximate solution obtained by restricting the rods to lie on three mutually orthogonal axes (the so-called XYZ model). The paper is concluded in Sec. VIII.

II. MODEL

A. Ideal self-assembly

We begin by considering an ideal gas of M monomers in a volume V and at temperature T, capable of reversible self-assembly into linear aggregates. For simplicity we assume that isolated monomers are hard spheres of radius a and that linear aggregates are hard spherocylinders, composed of a cylinder of radius a and length l with hemispherical end caps. Assuming that volume is conserved when a monomer joins an aggregate, the length of the cylinder is $l_\sigma=(\sigma-1)\Delta l$, where $\Delta l=4a/3$ and the aggregation number $\sigma=\{1,2,3,\ldots\}$ is the number of constituent monomers.

The population of particles is characterized by the distribution $s_\sigma(\Omega)d\Omega$, the mole fraction of aggregates with index σ and orientation Ω in the differential solid angle $d\Omega=\sin(\theta)d\theta d\phi$. It satisfies the normalization $\Sigma_\sigma\int d\Omega s_\sigma=1$. We use the angular bracket to denote the mean value of a quantity over this distribution:

$$\langle A\rangle=\sum_{\sigma=1}^{\infty}\int d\Omega\ s_\sigma(\Omega)A_\sigma(\Omega). \tag{1}$$

The mean aggregation number is $\langle\sigma\rangle$ and the total number of aggregates is $N=M/\langle\sigma\rangle$. The mole fraction of unpolymerized monomer is $4\pi s_1$.

In this section we neglect the nonideality due to hard-core repulsions. The Helmholtz free energy is then the sum of three terms

$$F_{\text{ideal}}=F_{\text{agg}}+F_0+\lambda\left(\sum_\sigma\int d\Omega s_\sigma-1\right). \tag{2}$$

The first term is a phenomenological description of rod assembly. We assume that assembly is isodesmic, i.e., that the free energy decreases by a fixed amount Φ_0 for each monomer-monomer contact in an aggregate

$$\frac{\beta F[T,V,M,\Phi_0;s_\sigma(\Omega)]_{\text{agg}}}{V}=-\Phi_0(m-n)$$
$$=-\Phi_0 m\left(1-\frac{1}{\langle\sigma\rangle}\right), \tag{3}$$

where $\beta=1/k_BT$, $m=M/V$ is the number density of monomers (including those in aggregates), and $n=N/V$ is the number density of aggregates. A positive Φ_0 favors aggregation. The second term in Eq. (2) includes the classical contributions due to translation and the entropy of mixing

$$\frac{\beta F[T,V,M;s_\sigma(\Omega)]_0}{V}$$
$$=\frac{m}{\langle\sigma\rangle}\left\{\ln\left(\frac{m\Lambda_1^3}{\langle\sigma\rangle}\right)-1+\sum_\sigma\int d\Omega s_\sigma\ln(4\pi s_\sigma)\right\}, \tag{4}$$

where $\Lambda_1=(\beta h^2/2\pi m)^{1/2}$ is the thermal wavelength of a monomer [20]. The third term uses the Lagrange multiplier λ to enforce the normalization of the distribution. Minimization of the free energy in Eq. (2) gives the ideal, isotropic distribution $s_\sigma=\exp(-\sigma/\langle\sigma\rangle)/4\pi\langle\sigma\rangle$ for $\langle\sigma\rangle\gg1$, where the mean polymerization is $\langle\sigma\rangle=(m\Lambda_1^3/4\pi)^{1/2}\exp(\Phi/2)$. This is a classical result consistent with the law of mass action [21].

B. Nonideal contribution to F

We assume the particles interact only through their hard-core excluded volume, so the nonideal contribution to the free energy comes exclusively from the configuration integral. There are no known exact results for the configuration integral of a polydisperse solution of N spherocylinders. We use the expression derived by Cotter and Wacker [8] using scaled particle theory (SPT) (note that the independent variable is N, not M)

$$\frac{\beta F[T,V,N,s_\sigma(\Omega)]_{\text{config}}}{V}$$
$$=n\left\{-\ln(1-v)+\frac{B}{2}\left(\frac{n}{1-v}\right)+\frac{C}{3}\left(\frac{n}{1-v}\right)^2\right\}, \tag{5}$$

$$B=8\pi a^3+6\pi a^2\langle l\rangle+4\Gamma, \tag{6}$$

$$C=4(2\pi a^3+\pi a^2\langle l\rangle)(\pi a^3+\pi a^2\langle l\rangle+\Gamma), \tag{7}$$

$$\Gamma=a\sum_{\sigma,\sigma'}\int d\Omega\ d\Omega' l_\sigma s_\sigma l_{\sigma'}s_{\sigma'}|\sin(\gamma)|, \tag{8}$$

where $\langle l\rangle=\Delta l(\langle\sigma\rangle-1)$ is the mean cylinder length, $v=n(4\pi a^3/3)\langle\sigma\rangle$ is the particle volume fraction, and γ is the opening angle between orientations Ω and Ω'. In polar coordinates

$$\cos(\gamma)=\cos(\theta)\cos(\theta')+\sin(\theta)\sin(\theta')\cos(\phi-\phi'). \tag{9}$$

Equation (5) has the following desirable properties. (i) For $l_\sigma=l\gg a$, it matches Onsager's second virial approximation for monodisperse rods [7]. (ii) For $l_\sigma=0$, it matches the well-known SPT and Perkus-Yevick results for hard spheres [22]. (iii) The second virial coefficient is exact. (iv) It compares well with the recent simulation results of Bolhuis and Frenkel for monodisperse rigid spherocylinders with aspect ratios $7\leqslant l/a\leqslant100$ [23]. Figure 1 shows a comparison of their isotropic-nematic coexistence concentrations with the second virial theory of Onsager and the scaled particle theory of Cotter and Wacker. There are no free parameters. Onsager's second virial approximation gives values that are too large by 20% at $l/a=50$ and does significantly worse for

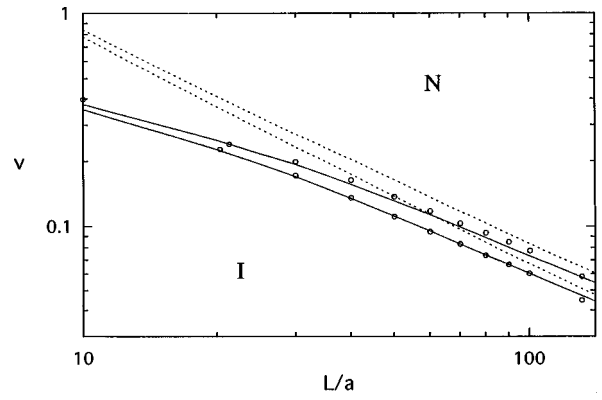

FIG. 1. Solute volume fractions at isotropic-nematic coexistence as a function of spherocylinder aspect ratio. *I* and *N* denote isotropic and nematic phases. Circles are simulation results of Bolhuis and Frenkel [23]. Solid lines are calculated using Eq. (5). Dashed lines are calculated using Onsager's second virial approximation.

smaller aspect ratios. The values obtained using Eq. (5) agree with the simulation results to 5% for $l/a>20$ and 10% for $10<l/a<20$.

In the case of reversible assembly, Eq. (5) is unchanged. However, the independent variable is the number of monomers M, rather than the number of spherocylinders N, so we need the relations $n=m/\langle\sigma\rangle$ and $v=(4\pi a^3/3)m$. The total free energy is then

$$F_{\rm tot}=F_0+F_{\rm config}+F_{\rm agg}+\lambda\left(\sum_\sigma \int d\Omega s_\sigma-1\right). \quad (10)$$

The remainder of this paper is concerned with finding the distribution $s_\sigma(\Omega)$ that minimizes $F_{\rm tot}$ and calculating the resulting thermodynamic quantities.

Taking the functional derivative $\delta F_{\rm tot}/\delta s_\sigma(\Omega)=0$ confirms that the equilibrium distribution has the functional form $s_\sigma(\Omega)=s_1 g(\Omega)^{\sigma-1}$, consistent with the law of mass action. The length and orientation distribution is fully specified by the function $g(\Omega)$. Strictly speaking, g is the dimer orientation distribution function, but for brevity we will refer to it as the distribution function since we seldom need to distinguish it from s_σ. Completing the sums over σ, the free energy becomes

$$\frac{\beta F_{\rm tot}}{V}=-m\Phi_0+n\left\{\Phi+\ln(4\pi s_1)+\Psi-1+\ln\left(\frac{na^3}{1-v}\right)+\frac{B}{2}\left(\frac{n}{1-v}\right)+\frac{C}{3}\left(\frac{n}{1-v}\right)^2\right\}, \quad (11)$$

where $\Phi=\Phi_0+3\ln(\Lambda_1/a)$ and the four integrals to be calculated are

$$s_1=\left(\int d\Omega\,\frac{1}{1-g(\Omega)}\right)^{-1}, \quad (12)$$

$$\langle\sigma\rangle=s_1\int d\Omega\,\frac{1}{[1-g(\Omega)]^2}, \quad (13)$$

$$\Psi=s_1\int d\Omega\,\frac{g(\Omega)\ln[g(\Omega)]}{[1-g(\Omega)]^2}, \quad (14)$$

$$\Gamma=a(s_1\Delta l)^2\int d\Omega\,\frac{g(\Omega)}{[1-g(\Omega)]^2}\times\int d\Omega'\,\frac{g(\Omega')}{[1-g(\Omega')]^2}|\sin(\gamma)|. \quad (15)$$

The Lagrange multiplier has been eliminated in favor of the normalization (12). The integrals may be simplified using the expected axial symmetry of the distribution $g(\Omega)=g(\theta)=g(\pi-\theta)$, so that

$$\int d\Omega\,A(g(\Omega))=4\pi\int_0^{\pi/2}d\theta\,\sin(\theta)A(g(\theta)) \quad (16)$$

and

$$\Gamma=a(4\pi s_1\Delta l)^2\int_0^{\pi/2}d\theta\,\sin(\theta)\,\frac{g(\theta)}{[1-g(\theta)]^2}\times\int_0^{\pi/2}d\theta'\sin(\theta')\,\frac{g(\theta')}{[1-g(\theta')]^2}W(\theta,\theta'), \quad (17)$$

$$W(\theta,\theta')\equiv\frac{1}{2\pi}\int_0^{2\pi}d\phi|\sin(\gamma)|. \quad (18)$$

The first term in Eq. (11), $-m\Phi_0$, changes only the zero of the chemical potential and has no effect on the distribution. For convenience we absorb this into the definition of $F_{\rm tot}$. The parameter Φ is twice the free energy cost per spherocylinder end cap, i.e., the cost to break a filament. The distribution depends only on the end cap energy Φ and the particle volume fraction v. It must be determined by minimizing $F_{\rm tot}$.

III. NUMERICAL SOLUTION FOR THE DISTRIBUTION FUNCTION

A. Numerical difficulties

In Ref. [19], Hentschke and Herzfeld derived an iterative equation for the distribution from the functional derivative $\delta F_{\rm tot}/\delta g=0$. The integrals in Eqs. (12)–(15) were solved by discretizing in the variable $x=\cos(\theta)$ and performing Gauss-Legendre integration [24]. They found good convergence in the thermodynamic variables and located the expected isotropic-nematic transition. However, in a similar calculation we found that the results depended sensitively on the angular resolution ϵ of the discretization. The apparent cause is that the distribution function exhibits approximately linear behavior $g\approx 1-\alpha\theta$ over a range $\theta_1<\theta<0.1$, before reaching a plateau at small θ. The cutoff θ_1 decreases rapidly with increasing concentration and may be many orders of magnitude smaller than 0.1. Since the integrals depend on $1/(1-g)$, special care must be taken near the origin. For example, if $\epsilon\gg\theta_1$ a calculation of $\langle\sigma\rangle$ finds

$$\langle\sigma\rangle=(4\pi s_1)\int_0^{\pi/2}d\theta\,\sin(\theta)\,\frac{1}{[1-g(\theta)]^2}\sim\int_\epsilon d\theta\frac{1}{\theta}\sim\ln(1/\epsilon) \quad (19)$$

rather than $\sim\ln(1/\theta_1)$. A numerical solution using a discretization of g must have a resolution of order θ_1 near the origin, while the resolution in Ref. [19] was $\epsilon\approx 0.02$.

A related problem is that a numerical solution with P digits of precision in g only has $P-\log_{10}(1/\theta_1)$ digits of precision in $1/(1-g)$. Even $P=32$ turns out to be inadequate for most cases of interest. In Secs. III B and III C we present an iterative scheme and a discretization that avoids these difficulties.

B. Iterative equation

The numerical precision lost when working with g is preserved if we instead work with the field $\eta\equiv\ln[g/(1-g)]$. The inverse transformation is $g=e^{\eta}/(1+e^{\eta})$. Note that while $0<g<1$, η is not bounded. This is an additional advantage since we will use an iterative procedure. The integrals in Eqs. (12)–(15) become

$$s_1=\left(\int d\Omega\ (1+e^{\eta})\right)^{-1}, \tag{20}$$

$$\langle\sigma\rangle=s_1\int d\Omega\ (1+e^{\eta})^2, \tag{21}$$

$$\Psi=s_1\int d\Omega\ (e^{\eta}+e^{2\eta})[\eta-\ln(1+e^{\eta})], \tag{22}$$

$$\Gamma=a(s_1\Delta l)^2\int d\Omega\ (e^{\eta}+e^{2\eta})\int d\Omega'(e^{\eta'}+e^{2\eta'})|\sin(\gamma)|, \tag{23}$$

where we have introduced the shorthand notation $\eta=\eta(\Omega)$ and $\eta'=\eta(\Omega')$. Taking a functional derivative of Eq. (11) with respect to η gives

$$0=-\frac{1}{\langle\sigma\rangle}\frac{\delta\langle\sigma\rangle}{\delta\eta}\hat{\Phi}-s_1e^{\eta}\Psi+s_1[\eta-\ln(1+e^{\eta})](e^{\eta}+2e^{2\eta})+\frac{1}{2}\frac{\delta B}{\delta\eta}\left(\frac{n}{1-v}\right)+\frac{1}{3}\frac{\delta C}{\delta\eta}\left(\frac{n}{1-v}\right)^2, \tag{24}$$

where

$$\hat{\Phi}=\Phi+\ln(4\pi s_1)+\Psi+\ln\left(\frac{na^3}{1-v}\right)+B\frac{n}{1-v}+C\left(\frac{n}{1-v}\right)^2, \tag{25}$$

$$\frac{\delta B}{\delta\eta}=6\pi a^2\Delta l\frac{\delta\langle\sigma\rangle}{\delta\eta}+4\frac{\delta\Gamma}{\delta\eta}, \tag{26}$$

$$\frac{\delta C}{\delta\eta}=(3\pi a^3+2\pi a^2\langle l\rangle+\Gamma)4\pi a^2\Delta l\frac{\delta\langle\sigma\rangle}{\delta\eta}+4(2\pi a^3+\pi a^2\langle l\rangle)\frac{\delta\Gamma}{\delta\eta}, \tag{27}$$

$$\frac{\delta\langle\sigma\rangle}{\delta\eta}=-s_1e^{\eta}\langle\sigma\rangle+2s_1(e^{\eta}+e^{2\eta}), \tag{28}$$

$$\frac{\delta\Gamma}{\delta\eta}=2(s_1\Delta l)^2(e^{\eta}+2e^{2\eta})\int d\Omega'(e^{\eta'}+e^{2\eta'})|\sin(\gamma)|. \tag{29}$$

Equation (24) is a nonlinear integral equation for η. It cannot be solved in closed form, but it may be used as the basis for an iterative solution

$$\eta=\ln(1+e^{\eta})+\frac{1}{s_1(e^{\eta}+2e^{2\eta})}\left[\frac{1}{\langle\sigma\rangle}\frac{\delta\langle\sigma\rangle}{\delta\eta}\hat{\Phi}+s_1e^{\eta}\Psi-\frac{1}{2}\frac{\delta B}{\delta\eta}\left(\frac{n}{1-v}\right)-\frac{1}{3}\frac{\delta C}{\delta\eta}\left(\frac{n}{1-v}\right)^2\right], \tag{30}$$

where the jth iterate $\eta^{(j)}$ is substituted into the right-hand side to generate $\eta^{(j+1)}$ on the left. Many different iterative equations can be derived from Eq. (24). We find empirically that Eq. (30) gives a monotonic decrease in the free energy with each iteration and has no spurious singular behavior.

C. Discretization

To solve the problem of resolution at small θ, discussed in Sec. III A, we convert to the logarithmic variable $u=-\ln(2\theta/\pi)$ and make a uniform discretization on u. The inverse transformation is $\theta=(\pi/2)\exp(-u)$. The integral over an axially symmetric function A becomes

$$\int_0^{\pi/2}d\theta\ \sin(\theta)A(\theta)=\int_0^{\infty}du\frac{\pi}{2}e^{-u}\sin\left(\frac{\pi}{2}e^{-u}\right)A(u). \tag{31}$$

This transformation is only useful if $A(u)$ goes to a constant $A(u\geqslant u_{\max})\approx A(u_{\max})$ for some $u_{\max}\gg 1$ [i.e., $A(\theta\leqslant\theta_{\min})\approx A(\theta_{\min})$ for $0<\theta_{\min}\ll 1$]. Then we can use the following approximate result at the upper limit of integration:

$$\int_{u_{\max}}^{\infty}du\frac{\pi}{2}e^{-u}\sin\left(\frac{\pi}{2}e^{-u}\right)A(u)\approx\int_{u_{\max}}^{\infty}du\left(\frac{\pi}{2}e^{-u}\right)^2A(u_{\max})=\frac{1}{2}\left(\frac{\pi}{2}e^{-u_{\max}}\right)^2A(u_{\max}). \tag{32}$$

The usual discretization on N_u equally spaced points is

$$\int_0^{u_{\max}}du\frac{\pi}{2}e^{-u}\sin\left(\frac{\pi}{2}e^{-u}\right)A(u)=\frac{\pi}{2}\Delta u\sum_{j=1}^{N_u}x_j'e^{-u_j}\sin\left(\frac{\pi}{2}e^{-u_j}\right)A(u_j), \tag{33}$$

where $u_j=(j-1)\Delta u$, $\Delta u=u_{\max}/(N_u-1)$, $x_1'=x_{N_u}'=1/2$, and $x_{j\neq 1,N_u}'=1$. Combining these results gives

$$\int_0^{\pi/2}d\theta\ \sin(\theta)A(\theta)=\Delta u\sum_{j=1}^{N_u}x_j\theta_j\sin(\theta_j)A(u_j), \tag{34}$$

where $x_1=1/2$, $x_{j\neq 1,N_u}=1$, $x_{N_u}=(1+1/\Delta u)/2$, and $\theta_j=(\pi/2)\exp(-u_j)$. In the numerical calculations discussed below, it must be verified *a posteriori* that all integrands are approximately constant near $u_{\max}$. The application of this

TABLE I. Solute volume fractions discussed in the text.

Φ	$\nu_{\min}$	ν_c	$\nu_{\mathrm{UB}}^{\mathrm{it}}$	$\nu_{\mathrm{UB}}^{4\,\mathrm{par}}$
3	0.352	0.358	0.370	0.389
10	0.083	0.084	0.103	0.114

discretization to Eqs. (20)–(22) is straightforward, but Eqs. (23) and (29) have an additional complication due to the term $|\sin(\gamma)|$:

$$\Gamma = a(4\pi s_1 \Delta l \Delta u)^2 \sum_{i=1}^{N_u} x_i \theta_i \sin(\theta_i) h_i \times \sum_{j=1}^{N_u} x_j \theta_j \sin(\theta_j) h_j W_{ij}, \tag{35}$$

$$\frac{\delta\Gamma}{\delta\eta}(u_i) = 2(s_1\Delta l)^2 (e^{\eta_i} + 2e^{2\eta_i}) 4\pi\Delta u \times \sum_{j=1}^{N_u} x_j \theta_j \sin(\theta_j) h_j W_{ij}, \tag{36}$$

where $\eta_i = \eta(u_i)$, $h_i = \exp(\eta_i) + \exp(2\eta_i)$ and W_{ij} is the discretized kernel [see Eq. (18)]

$$W_{ij} = \Delta\phi \sum_{k=1}^{N_\phi} |\sin[\gamma(\theta_i, \theta_j, \phi_k)]|, \tag{37}$$

with $\phi_k = k\Delta\phi$ and $\Delta\phi = 2\pi/N_\phi$. We take $N_\phi = 1024$. It is convenient to calculate and store the values of W_{ij} prior to iterating Eq. (30).

We typically use $N_u = 128$ points. As discussed in the next subsection, the accuracy was checked by comparing with the results for $N_u = 64$. We also verified that the results were independent of the value of $u_{\max}$ over the range $10 \leqslant u_{\max} \leqslant 24$. Our criterion for convergence is that the change in η is less than 10^{-8} per iteration.

D. Results

Since the iterative scheme is explicitly a single-phase calculation, we reserve the discussion of phase coexistence until Sec. VI. In this section the ''stable phase'' refers to the single (isotropic or nematic) phase that has the lowest free energy at a given volume fraction. This should not be confused with global thermodynamic stability.

As expected, the iterative scheme converges to an isotropic phase at low volume fractions and a nematic phase at high volume fractions. There is also a considerable range over which either phase may be found, depending on the initial choice for g. Table I shows some representative values of the volume fraction for $\Phi = 3$ and $\Phi = 10$. The minimum volume fraction for which we could find a nematic phase is $v_{\min}$. The volume fraction at which the isotropic and nematic free energies are equal is v_c, so the nematic phase is metastable for $v_{\min} \leqslant v \leqslant v_c$. Above v_c the isotropic phase is metastable. Near v_c, the basin of attraction for the isotropic phase is large, so convergence to a nematic distribution requires a sharply peaked initial condition such as $g^{(0)} = 0.3 + 0.699 \exp(-3\theta)$.

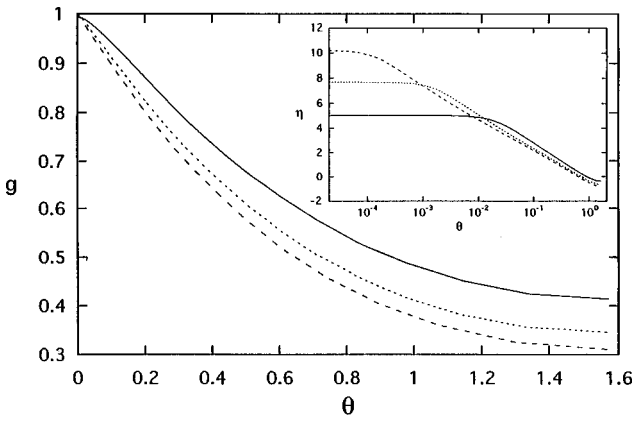

FIG. 2. Nematic distribution function calculated at three different solute volume fractions: $v = 0.352$ (—), $v = 0.358$ (···), and $v = 0.365$ (- - -), with $\Phi = 3$. The inset shows η to emphasize the small-angle behavior.

In the isotropic phase convergence requires fewer than 200 iterations ($\sim$2 sec on an IBM RS/6000 computer). The resulting distribution function is approximately constant, with small systematic deviations due to the finite resolution of the discretization. For $N_u = 64$ and $u_{\max} = 24$, the deviations are of relative magnitude $\sim 0.1\%$. Increasing the number of points to $N_u = 128$ or decreasing $u_{\max}$ to 10 decreases the magnitude of the deviations to $\sim 0.01\%$.

We make a further check on the accuracy of our isotropic phase results using the following calculation. In the isotropic phase $g(\theta) = g_I$ and the integrals in Eqs. (12)–(15) can be solved exactly,

$$s_1 = \frac{1 - g_I}{4\pi}, \quad \langle\sigma\rangle = \frac{1}{1 - g_I}, \quad \Psi = \frac{g_I \ln(g_I)}{1 - g_I}, \tag{38}$$

$$\Gamma = \frac{\pi}{4} a \Delta l^2 (\langle\sigma\rangle - 1)^2.$$

Substituting into Eq. (11) gives $F_{\mathrm{tot}}[T,V,M,\Phi;g_I]$. We then find the value of g_I that minimizes F_{tot} using a downhill simplex minimization routine [24]. This allows us to calculate all quantities with a relative accuracy of 10^{-8}. A comparison with the results of the iterative scheme shows that the discretization using $N_u = 64$ and $u_{\max} = 24$ gives values of g_I and F_{tot} that are too large by $\sim 1\%$. Halving Δu improves agreement to $\sim 0.1\%$.

In the nematic phase, we can only find a converged distribution at volume fractions near v_c. Figure 2 shows the distributions g and η for three values of v at $\Phi = 3$. The distribution g is distinctly non-Gaussian. Note the approximately linear approach to 1 at small θ, with a cutoff that decreases exponentially with the volume fraction. At $v_c = 0.358$, $\theta_1 \approx 0.002$. This illustrates the problem discussed in Sec. III A. It would be impractical to resolve the cutoff using a uniform discretization in θ.

The number of iterations needed to find convergence of the nematic distribution grows exponentially with increasing solute volume fraction. After about $j = 1000$ iterations the

general shape of $g(\theta)$ is well established, including the linear regime and a plateau at small θ, but the cutoff is typically much larger than its converged value. The main effect of further iteration is to decrease the value of the cutoff, approximately as $\theta_1^{(j)} \approx 0.01/j^{1/2}$, until it reaches a true limiting value. The problem arises because the limiting value decreases exponentially with increasing volume fraction $\theta_1^{(\infty)} \sim 10^{-170v}$ (see Fig. 2). The number of iterations needed for the plateau to achieve its asymptotic form therefore increases exponentially with volume fraction. Choosing a limit on CPU time of about 1 day gives a practical upper bound $v_{\mathrm{UB}}^{\mathrm{it}}$, on the volume fractions for which the nematic distribution function can be determined. Values of $v_{\mathrm{UB}}^{\mathrm{it}}$ for $\Phi=3$ and $\Phi=10$ are listed in Table I. We see that the iterative scheme converges over a range of only 0.02 in volume fraction, independent of v_c. Attempts to speed convergence using an initial condition that anticipates the smallness of the cutoff show only modest gains in speed.

In the nematic phase, the free energy converges significantly faster than the distribution function. As a result, F_{tot} can be reliably determined for volume fractions greater than $v_{\mathrm{UB}}^{\mathrm{it}}$ by as much as 0.25, typically after 10^4 iterations [see Fig. 6(b) below]. At still higher concentrations, F_{tot} converges too slowly and we need a new method of solution. In the next section we introduce a trial function to approximate the distribution g. The trial function approach is much faster than the iterative scheme and it allows us to minimize F_{tot} over the full range of volume fractions. It also clarifies the problems of convergence encountered in this section (see Sec. IV B).

IV. TRIAL FUNCTION FOR THE DISTRIBUTION

A. Trial function and approximate *W*

We seek an alternative to the iterative scheme of Sec. III. To this end we present a trial function for g,

$$g(\theta)=\begin{cases} 1-\alpha R\,\sin(\theta_1)=g_0, & 0\leqslant\theta\leqslant\theta_1 \\ 1-\alpha\,\sin(\theta), & \theta_1\leqslant\theta\leqslant\theta_2 \\ 1-\alpha\,\sin(\theta_2)=g_2, & \theta_2\leqslant\theta\leqslant\pi/2, \end{cases} \tag{39}$$

where we require $0<g_0$ and $g_2<1$. This expression has four free parameters $\{\alpha,R,\theta_1,\theta_2\}$. It was chosen because it captures all the important qualitative features of the nematic distribution, including an approximately linear approach to 1 and a plateau at small angles. We will see that $R<1$ in the nematic phase, so g is discontinuous at θ_1. Attempts to eliminate any one of the parameters (e.g., by setting $R=1$ or $\theta_1=\theta_2$) lead to poor agreement with the distributions found in Sec. III. The trial function was also chosen to make Eqs. (12)–(14) almost completely integrable in terms of elementary functions. The resulting expressions are presented in Appendix A.

The most computationally intensive term in the free energy is Eq. (17), the two-dimensional integral for Γ. Here we make an analytic approximation for the kernel W [see Eq. (18)] which, in combination with the trial function, simplifies Eq. (17) considerably. In the domain $0\leqslant\theta'\leqslant\theta\leqslant\pi/2$, we approximate

$$\tilde{W}(\theta,\theta')=\sin(\theta)\left(1+c\,\frac{\sin^2(\theta')}{4\sin^2(\theta)}[1-2\sin^2(\theta)]\right), \tag{40}$$

where $c=1.3$. This form is suggested by the Taylor series for W in powers of $\sin(\theta')$, given by $c=1$ and derived in Appendix B. A comparison of $\tilde{W}$ with W using MATHEMATICA (Wolfram Media, Cambridge) shows that the relative error of Eq. (40) is less than 7% over the whole domain. In Appendix C we solve Eq. (17) in terms of elementary functions of $\{\alpha,R,\theta_1,\theta_2\}$, with the exception of one one-dimensional integral to be calculated numerically.

The trial function solution requires the minimization of F_{tot} with respect to the four parameters $\{\alpha,R,\theta_1,\theta_2\}$ at fixed v and Φ. We use a downhill simplex minimization routine [24]. At low volume fractions we recover the isotropic distribution characterized by $\theta_1=\theta_2$, $R=1$, and $g_I=1-\alpha\,\sin(\theta_1)$. The value of g_I is not identical to the value found in Sec. III D due to the approximation used here for W, but the resulting errors in $\langle\sigma\rangle$ and F_{tot} are $\sim 0.1\%$ and $\sim 0.01\%$ respectively. The main advantage of the trial function is in the treatment of the nematic phase. When convergence can be found (see below), the algorithm requires about 0.1 sec of CPU time.

B. Determination of *R* and θ_1 in the nematic phase

Our first attempts to minimize F_{tot} with respect to the four parameters $\{\alpha,R,\theta_1,\theta_2\}$ depended sensitively on the numerical precision of the calculation. To understand this sensitivity, we expand the expressions in Appendixes A and C for s_1, $\langle\sigma\rangle$, Ψ, and Γ to leading order in θ_1. Each has the form

$$I(\alpha,R,\theta_1,\theta_2)=I_0\left(\alpha,\theta_2,\zeta=-\ln(\theta_1)+\frac{1}{2R^2}\right) + \theta_1 I_1(\alpha,R,\theta_1,\theta_2). \tag{41}$$

As a result, the independent determination of R and θ_1 requires a precision of order θ_1. This does not pose a difficulty near v_c, but θ_1 decreases exponentially with increasing volume fraction. Table I lists the approximate upper bound $v_{\mathrm{UB}}^{4\,\mathrm{par}}$ on the range of volume fractions accessible to the four-parameter solution at $\Phi=3$ and $\Phi=10$. Even with 32 significant figures, R and θ_1 can only be independently determined over a range of about 0.03 in volume fraction. Outside this range, numerical techniques can only reliably determine the three parameters $\{\alpha,\zeta,\theta_2\}$. We do not consider this to be a prohibitive drawback since the integrals in Appendixes A and C, and hence the free energy, can be determined to high precision over the full range of volume fractions $0<v<1$.

These observations may help clarify the slow convergence of the iterative solution in Sec. III. For the trial function, one value of ζ parametrizes a large set of distributions that differ only in their small-θ behavior and whose free energies are within order θ_1 of each other. In other words, the free energy landscape in $\{R,\theta_1\}$ has a narrow valley whose floor has a very shallow slope. The same is apparently true for the exact solution. The relatively rapid convergence

of $F_{\rm tot}$ in Sec. III finds the valley. The slow convergence of the distribution is due to the shallow slope within the valley.

If values for $\{R,\theta_1\}$ are desired for $v>v_{\rm UB}^{4\,\rm par}$, we can take advantage of the analytic form for the free energy in terms of the trial function parameters. We need the value of R that satisfies (note the change of independent variables)

$$\frac{\partial}{\partial R}F_{\rm tot}(\alpha,R,\zeta,\theta_2)=0. \tag{42}$$

From Eq. (41) we see that the derivative is proportional to θ_1. Using the expressions in Appendixes A and C we could calculate the derivative to leading order in θ_1, divide out θ_1, and find the root using standard methods. The full calculation would be too long to attempt here. Instead, we take advantage of the following observation. In the range of volume fractions where we can determine θ_1 and R independently, the minimum of $F_{\rm tot}$ coincides approximately with the minimum

$$\frac{\partial}{\partial R}\Gamma_0(\alpha,R,\zeta,\theta_2)=0, \tag{43}$$

where Γ_0 is the contribution to Γ due to the leading-order term in the Taylor series of W [set $c=0$ in Eq. (40); see the Appendixes].

We therefore propose the following algorithm for the independent determination of R and θ_1. (i) Given values for Φ and v, fix $R=1$ and minimize $F_{\rm tot}$ with respect to the three parameters $\{\alpha,\zeta,\theta_2\}$. From Eq. (41) we expect that the parameters and the free energy found in this way will have an error of order θ_1. (ii) Solve Eq. (43) for R using the values for $\{\alpha,\zeta,\theta_2\}$ found in step (i). Then $\theta_1=\exp(-\zeta+1/2R^2)$. Although this only provides approximate values for R and θ_1, it has a significant advantage. Step (ii) can be done *analytically*. Writing $\Gamma_0=a(4\pi s_1\Delta l)^2 I$ (see Appendix C), Eq. (43) is

$$0=\frac{\partial}{\partial R}\Gamma_0(\alpha,R,\zeta,\theta_2)=a(4\pi\Delta l)^2\left(2s_1\frac{\partial s_1}{\partial R}I+s_1^2\frac{\partial I}{\partial R}\right), \tag{44}$$

$$\frac{\partial}{\partial R}s_1(\alpha,R,\zeta,\theta_2)=2\pi s_1^2\frac{e^{-\zeta+1/2R^2}}{\alpha R^4}(1-R)^2, \tag{45}$$

$$\frac{\partial}{\partial R}I(\alpha,R,\zeta,\theta_2)=-\frac{e^{-\zeta+1/2R^2}}{5\alpha^4R^7}(1-R^2)+\frac{e^{-\zeta+1/2R^2}}{2R^4}(1-R)^2 f, \tag{46}$$

$$f=\frac{2}{\alpha^3}[\theta_2-\alpha+\alpha\cos(\theta_2)]+\frac{g_2}{\alpha(1-g_2)^2}\left(\frac{\pi}{2}-\theta_2+\frac{\sin(2\theta_2)}{2}\right). \tag{47}$$

Substituting Eqs. (45)–(47) into Eq. (44) and eliminating common terms gives

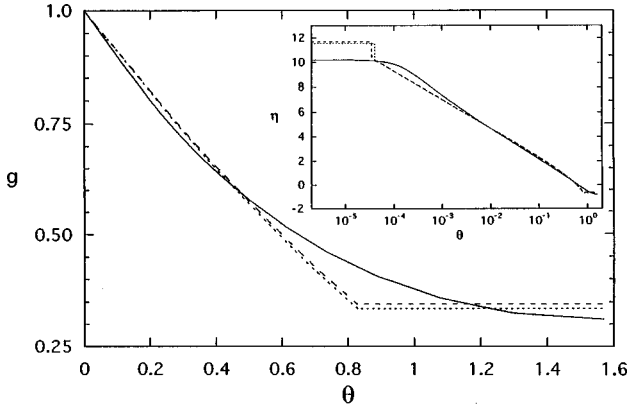

FIG. 3. Nematic distribution function at $v=0.365$ and $\Phi=3$, calculated using the iterative scheme of Sec. III (—), the four-parameter trial function (···), and the $(3+1)$-parameter trial function (---).

$$c_-R^3(1-R)-c_+(1+R)=0,\qquad c_+=\frac{1}{5\alpha^4},\quad c_-=\frac{4\pi s_1 I}{\alpha}+\frac{f}{2}. \tag{48}$$

The quartic polynomial in R can be solved exactly. It has two real roots, but only one corresponds to the minimum of Γ_0:

$$R=\frac{1}{4}+\frac{b_1^{1/2}}{2}-\frac{1}{2}\sqrt{\frac{3}{4}+\frac{1-8c_+/c_-}{4b_1^{1/2}}-b_1}, \tag{49}$$

$$b_1=\frac{1}{4}+\frac{5c_+}{3b_2^{1/3}}+\frac{b_2^{1/3}}{c_-}, \tag{50}$$

$$b_2=\frac{c_+c_-}{2}\left(c_++c_-+\sqrt{c_+^2+c_-^2-\frac{446}{27}c_+c_-}\right). \tag{51}$$

This is our prescription for R in terms of $\{\alpha,\zeta,\theta_2\}$. We will refer to this as the $(3+1)$-parameter solution to distinguish it from the four-parameter solution, in which we minimize $F_{\rm tot}$ with respect to $\{\alpha,R,\theta_1,\theta_2\}$.

C. Results

In this section we present representative results, obtained for $\Phi=3$. Figure 3 shows a comparison of the nematic distribution function derived in Sec. III to the results of the four-parameter and $(3+1)$-parameter calculations, all at $v=0.365$. We see good qualitative agreement between all three. In particular, the linear approach to 1 and the plateau at small θ are well represented.

Figure 4 shows the trial function parameters as a function of volume fraction in the nematic phase, calculated using the $(3+1)$-parameter solution. The most surprising feature is the enormous range of θ_1 values, 10^{-3}–$10^{-10^{18}}$. This is the source of the numerical difficulties discussed above.

It is instructive to compare the results of the $(3+1)$-parameter solution to the four-parameter solution over the limited range of volume fractions where the latter can be accurately determined. At $\Phi=3$, the minimum volume fraction for which a nematic phase can be found is

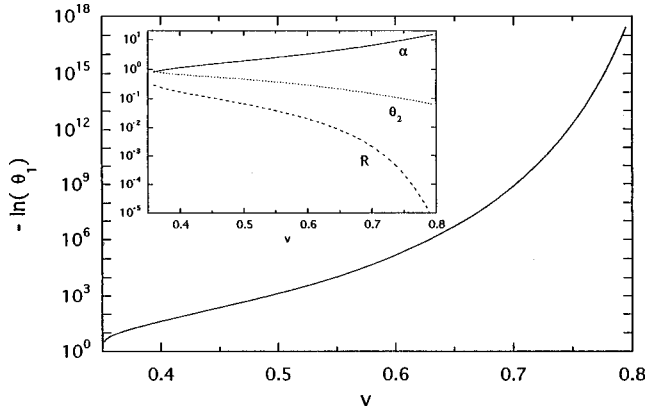

FIG. 4. Four trial function parameters versus solute volume fraction at $\Phi=3$, calculated using the $(3+1)$-parameter solution.

$v_{\min}=0.352$ and the upper bound on the four-parameter solution due to numerical limitations is $v_{\mathrm{UB}}^{4\,\mathrm{par}}=0.389$. Within this range the free energies differ by less than 1%. Figure 5(a) compares the values of the trial function parameters α, θ_2, and R. Agreement is typically within a few percent, although the R values differ by as much as 11%. Figure 5(b) compares the values of θ_1. Since $\theta_1 \sim \exp(1/2R^2)$ at fixed ζ, we find much larger differences in the values of θ_1. It should be noted that the θ_1 values found using the $(3+1)$-parameter solution are still orders of magnitude more accurate than those found using the arbitrary choice $R=1$.

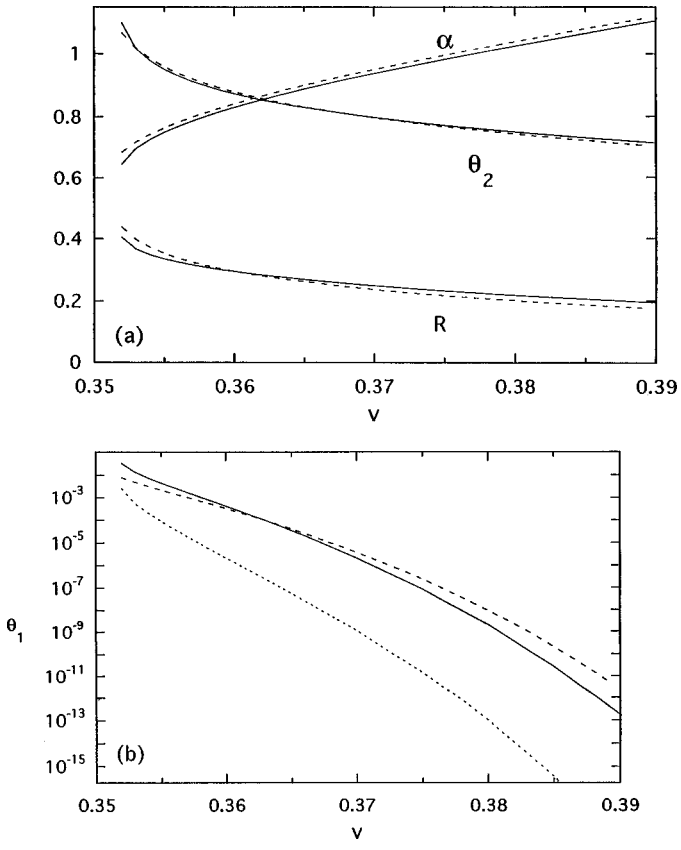

FIG. 5. Trial function parameters versus solute volume fraction at $\Phi=3$, calculated using the four-parameter solution (—), the $(3+1)$-parameter solution (---), and the three-parameter solution found by setting $R=1$ $(\cdots)$.

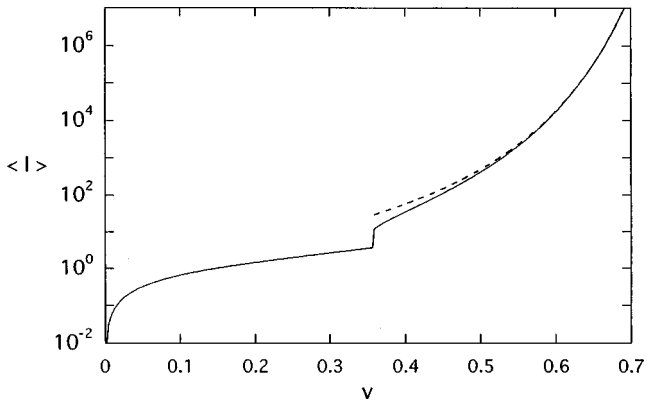

FIG. 6. Mean cylinder length versus solute volume fraction at $\Phi=3$, calculated using the $(3+1)$-parameter solution (—) and the approximate solution derived in Sec. V (---). Note the isotropic-nematic crossover.

Figures 6 and 7 show further results for the $(3+1)$-parameter solution. The value of the isotropic-nematic crossover is $v_c=0.358$, within 0.01% of the value found in Sec. III. Figure 6 shows the mean cylinder length $\langle l\rangle=\Delta l(\langle\sigma\rangle-1)$ versus volume fraction. At v_c the length increases abruptly from $3.7a$ to $11.9a$, in agreement with the expectation that orientational ordering decreases the steric hindrance to polymerization (Refs. [13] and [25] found qualitatively similar results). The mean length increases faster than exponentially with increasing volume fraction and diverges at $v=1$. Figure 7 shows the free energy versus solute volume fraction. F_{tot} asymptotically approaches 0 at $v=1$ because the number density of spherocylinders $n\sim v/\langle\sigma\rangle$ approaches 0. The inset of Fig. 7 compares the free energy results of the $(3+1)$-parameter trial function to the results of the iterative scheme after 1000, 3000, and 10 000 iterations. It is clear that the iterative scheme is converging to the $3+1$ values. After 3000 iterations the difference is less than 2% for $v<0.55$. These observations give us confidence in the accuracy of the $(3+1)$-parameter solution.

V. APPROXIMATE RESULTS FOR $V\rightarrow 1$

We can use the trial function results to motivate a useful simplification of the free energy (11) at high volume frac-

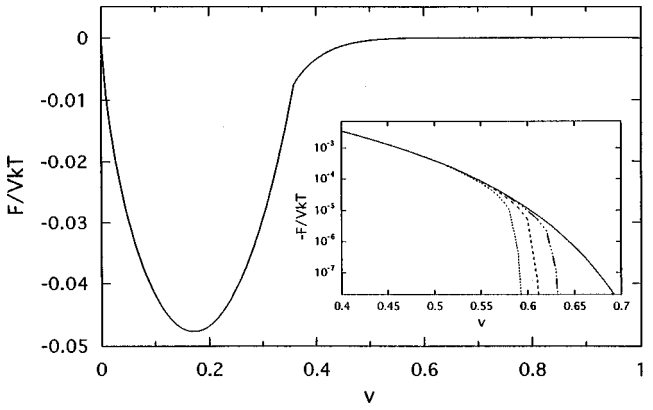

FIG. 7. Free energy versus solute volume fraction at $\Phi=3$ calculated using the $(3+1)$-parameter solution. Isotropic-nematic crossover at $v_c=0.358$. Inset: comparison in the nematic phase to the results of the iterative scheme after 10^3 $(\cdots)$, 3×10^3 (---), and 10^4 (—$\cdots$) iterations.

tions. As mentioned above, the mean length $\langle l\rangle$ grows without bound as $v\to 1$. We also find that $\Gamma/(a^2\langle l\rangle)\to 0$. Referring to the definition of Γ in Eq. (8), this implies that the rods are nearly parallel. These two conditions allow us to simplify the coefficients in the configuration integral [Eqs. (6) and (7)] to $B\to 6v/n$ and $C\to 4(v/n)^2$, where we have used the fact that $\pi a^2\langle l\rangle\to v/n$. We also find empirically that the orientational entropy per rod, $\ln(4\pi s_1)+\Psi$ in Eq. (11), tends toward zero with increasing volume fraction. These observations suggest the approximate free energy

$$\frac{\beta\tilde{F}_{\rm tot}[T,V,M,\Phi;n]}{V} = n\left\{\Phi-1+\ln\left(\frac{na^3}{1-v}\right)+3\left(\frac{v}{1-v}\right)+\frac{4}{3}\left(\frac{v}{1-v}\right)^2\right\}, \tag{52}$$

which we expect to be accurate at high volume fractions. (We will consistently use a tilde to distinguish the approximate results derived in this section.) Note that $\tilde{F}_{\rm tot}$ depends on the distribution only through the spherocylinder number density $n=m/\langle\sigma\rangle$.

Equation (52) illustrates the competing terms that determine n. The end cap energy Φ and the excluded volume terms favor a low number density n and therefore a high mean polymerization. The only term that favors a high n is the entropy of mixing, which enters $\tilde{F}_{\rm tot}$ as $n\{\ln(na^3)-1\}$.

We can find approximate closed form expressions for $F_{\rm tot}$ and n by minimizing Eq. (52) with respect to n. Solving $d\tilde{F}_{\rm tot}/dn=0$ gives

$$\tilde{n}=\left(\frac{1-v}{a^3}\right)\exp\left[-\Phi-3\left(\frac{v}{1-v}\right)-\frac{4}{3}\left(\frac{v}{1-v}\right)^2\right] \tag{53}$$

and $\beta\tilde{F}_{\rm tot}/V=-\tilde{n}$. Note that $\tilde{n}\to 0$ as $v\to 1$. These expressions show excellent agreement with the trial function results for $\Phi=3$ and $\Phi=10$ (see Sec. IV). The plot of mean cylinder length in Fig. 6 is typical. The error is about 20% at $v=0.5$ and less than 1% for $v\geq 0.7$. The closed expressions seem to be exact as $v\to 1$.

VI. THERMODYNAMIC QUANTITIES

A. Definitions

Once the distribution function has been found, we can calculate all the thermodynamic quantities of interest. In particular, the pressure is

$$\beta p=-\frac{\partial}{\partial V}\beta F_{\rm tot}[T,V,M,g(\theta)] = \frac{n}{1-v}+\frac{B}{2}\left(\frac{n}{1-v}\right)^2+\frac{2C}{3}\left(\frac{n}{1-v}\right)^3, \tag{54}$$

and the monomer chemical potential is

$$\beta\mu=\frac{\partial}{\partial M}\beta F_{\rm tot}[T,V,M,g(\theta)]=\frac{1}{M}(\beta F_{\rm tot}+\beta pV). \tag{55}$$

We define the reduced chemical potential $\mu^*=\beta\mu$ and the reduced pressure $p^*=\beta pV_1$, where $V_1=4\pi a^3/3$ is the volume of a monomer.

There are two ways of defining an order parameter for polydisperse systems. The number-averaged order parameter is

$$S_n=\sum_{\sigma=1}^{\infty}\int d\Omega\ s_\sigma(\Omega)P_2[\cos(\theta)] = 4\pi s_1\int_0^{\pi/2}d\theta\ \sin(\theta)\frac{1}{1-g(\theta)}P_2[\cos(\theta)], \tag{56}$$

and the mass-averaged order parameter is

$$S_m=\frac{1}{\langle\sigma\rangle}\sum_{\sigma=1}^{\infty}\sigma\int d\Omega\ s_\sigma(\Omega)P_2[\cos(\theta)] = \frac{4\pi s_1}{\langle\sigma\rangle}\int_0^{\pi/2}d\theta\ \sin(\theta)\frac{g(\theta)}{[1-g(\theta)]^2}P_2[\cos(\theta)], \tag{57}$$

where $P_2(x)=(3x^2-1)/2$ is the second-order Legendre polynomial. Birefringence studies measure S_m. Substitution of the trial function gives

$$S_n=\frac{\pi s_1}{\alpha}\left\{(\theta_2-\theta_1)+\left(\frac{1}{R}-\frac{3}{2}\right)\sin(2\theta_1)+\frac{1}{2}\sin(2\theta_2)\right\}, \tag{58}$$

$$S_m=\frac{4\pi s_1}{\alpha^2\langle\sigma\rangle}\left\{\left(\frac{1}{2R^2}-\frac{3}{2}\right)\cos(\theta_1)+\cos(\theta_2)+\ln\left(\frac{\tan(\theta_2)}{\tan(\theta_1)}\right)\right\}. \tag{59}$$

B. Results

We again pick the representative value $\Phi=3$. Figure 8(a) shows the reduced pressure versus solute volume fraction. The $(3+1)$-parameter solution is accurate over the whole range. We see a large drop in the pressure at the crossover to the nematic phase $v_c=0.358$. The iterative solution after 10 000 iterations differs from the $(3+1)$-parameter solution by less than 2% for $v\lesssim 0.55$. The approximate free energy derived in Sec. V gives an estimate for the pressure that is accurate to about 25% at $v=0.5$ and better than 1% for $v\geq 0.7$. Note that the pressure decreases monotonically to zero as the volume fraction increases, implying that the entire nematic phase is thermodynamically unstable. This behavior will be discussed in the next subsection. Figure 8(b) shows S_m and S_n in the nematic phase. The mass-averaged order parameter goes rapidly to 1 with increasing volume fraction. Surprisingly, the number-averaged order parameter remains small and decreases toward 0. This is another consequence of the increasing sharpness of g.

C. Singularity at $v=1$

The free energy (11) has a singularity at $v=1$, as do all scaled particle treatments. A more accurate free energy would presumably diverge at or below the close-packed volume fraction, but this should not make a qualitative differ-

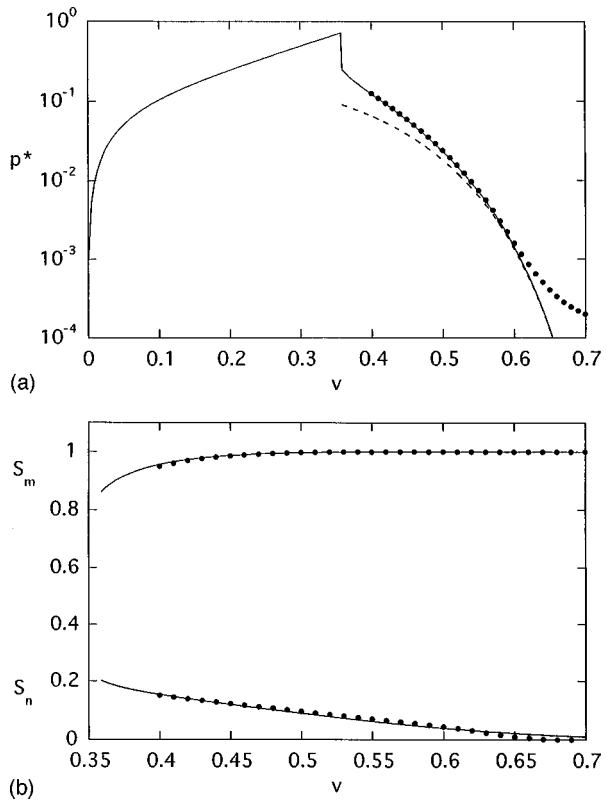

FIG. 8. (a) Reduced pressure and (b) mass-averaged and number-averaged order parameters versus solute volume fraction at $\Phi=3$, calculated using the $(3+1)$-parameter solution (—), the iterative scheme after 10^4 iterations (•), and the approximate solution of Sec. V (---).

ence in the resulting phase diagram. In this paper we assume that the solute volume fraction can increase to $v=1$.

The two conditions for phase coexistence are equality of pressures $p(I)=p(N)$ and chemical potentials $\mu(I)=\mu(N)$. Phase coexistence will therefore appear as an intersection on a plot of chemical potential versus pressure. Figure 9 shows the reduced chemical potential versus the reduced pressure for $\Phi=3$. The solid line, calculated for $v<1$, shows no intersection. The singularity provides the missing branch of the nematic pressure curve. We therefore expect to find coexistence between an isotropic phase with volume fraction $v(I)<v_c$ and a nematic phase with $v(N)=1$.

To find the contribution to the pressure due to the singularity at $v=1$, we make a careful treatment of the thermodynamic limits $V\to\infty$ and $M\to\infty$. Consider the limiting expression for the pressure (54) as $v\to 1$. From the results of Sec. V we have

$$\beta p \overset{v\to 1}{\sim} n\,\frac{8/3}{(1-v)^3}. \tag{60}$$

We see that $p\to 0$ as $v\to 1$ is a consequence of the fact that $n\to 0$ faster than $(1-v)^{-3}$ diverges. For an infinite box, there is no limit to this trend. However, in a cubic box of side L, the number of rods cannot decrease below $L^2/(\pi a^2)$, so $n\geqslant 1/\pi a^2 L$. Therefore,

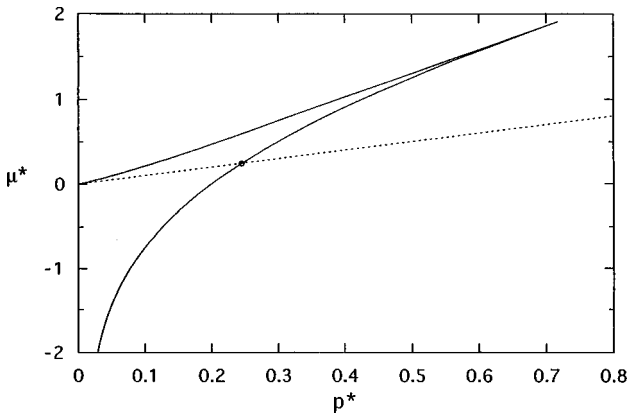

FIG. 9. Reduced chemical potential versus pressure at $\Phi=3$. The solid line is calculated away from the singularity at $v=1$. The dotted line is the contribution from the perfect nematic phase at $v=1$. The circle labels I-N coexistence at $\mu^*=p^*=0.245$.

$$\beta p \overset{v\to 1}{\sim} \frac{1}{\pi a^2 L}\,\frac{8/3}{(1-v)^3}, \tag{61}$$

which diverges at $v=1$. A similar calculation gives

$$\beta\mu \overset{v\to 1}{\sim} \frac{4a}{3L}\,\frac{8/3}{(1-v)^3}=\beta p V_1. \tag{62}$$

These expressions depend on the box size and are only significant for $1-v\lesssim(a/L)^{1/3}$, but the plot of chemical potential versus pressure is $\beta\mu=\beta pV_1$ *independent* of the box size. We show in Appendix D that this expression is valid for any sufficiently steep increase in the pressure. It does not depend on the specific form of the free energy.

The branch $\beta\mu=\beta pV_1$ appears as the dotted line in Fig. 9. We see that the isotropic phase coexists with a perfect nematic phase at $\mu^*=p^*=0.245$. The volume fraction of the isotropic phase is $v(I)=0.199$. We have repeated this calculation for a range of end cap energies Φ. Figure 10 shows the resulting phase diagram. As expected, an increase in Φ promotes the assembly of longer rods and favors the nematic phase.

VII. RESTRICTED ORIENTATION APPROXIMATION

The problem of self-assembling rods has often been simplified by restricting the rod orientations to three mutually orthogonal axes (often called the XYZ model) [26,27]. One can convert our free energy (Sec. II) to an XYZ model by discretizing the angular integrations

$$\int d\Omega A(g(\Omega))\to\frac{4\pi}{6}\sum_{i=\{\pm\hat{x},\pm\hat{y},\pm\hat{z}\}}A(g_i)$$
$$=\frac{4\pi}{6}\{2A(g_\perp)+4A(g_\parallel)\}, \tag{63}$$

$$\Gamma\to a\left(\frac{4\pi}{6}s_1\Delta l\right)^2\left\{16\,\frac{g_\parallel}{(1-g_\parallel)^2}\,\frac{g_\perp}{(1-g_\perp)^2}+8\,\frac{g_\perp^2}{(1-g_\perp)^4}\right\}, \tag{64}$$

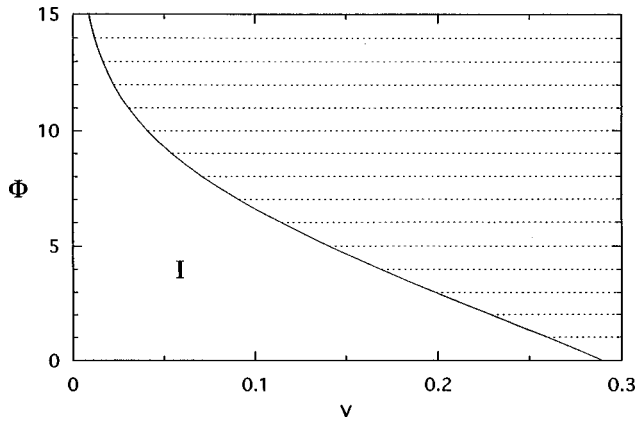

FIG. 10. *I-N* phase diagram as a function of solute volume fraction and end cap energy cost. *I* denotes the isotropic phase. Dotted tie lines connect the isotropic phase with the coexisting nematic phase at $v=1$.

where the sum over the six directions has been simplified using the expected axial symmetry of the solution. The values $g_{\|}$ and $g_{\perp}$ are taken parallel and perpendicular to the nematic director, respectively. To solve we specify Φ and v and use a downhill simplex routine to minimize F_{tot} with respect to $g_{\|}$ and $g_{\perp}$.

Figure 11 shows a comparison of the pressures for the *XYZ* model and the $(3+1)$-parameter trial function at $\Phi=10$. The positions of the isotropic phase boundaries compare well, but we otherwise see qualitative disagreement. The restricted orientation model underestimates the pressure by a factor of 4. Also note the second phase transition from a dilute nematic phase to a dense nematic phase predicted by the *XYZ* model. The nematic-nematic transition occurs for all $\Phi>8.5$. For values of $\Phi<8.5$, there is improved agreement between the *XYZ* and $(3+1)$-parameter results. There is a single phase transition from an isotropic phase to the nematic phase at $v(N)=1$. The pressure is still underestimated by about 30% at $\Phi=3$.

Qualitatively similar behavior was found by Herzfeld and co-workers in their theoretical studies of amphiphile self-assembly. Herzfeld and Taylor used a restricted orientation model and found a nematic-nematic transition, in addition to the expected isotropic-nematic transition, over a limited range of Φ values [28]. Hentschke and Herzfeld repeated the calculation using a continuum of orientations and found no nematic-nematic transition [19].

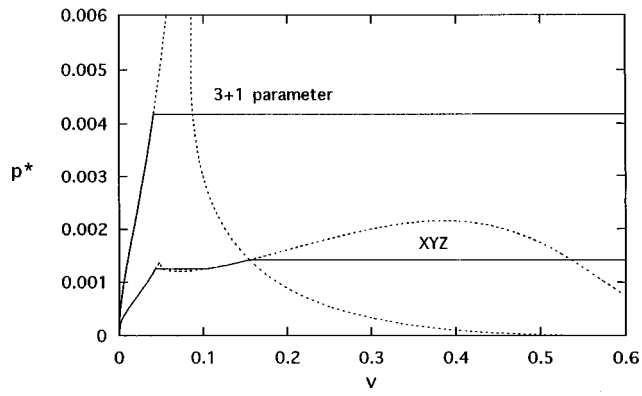

FIG. 11. Reduced pressure versus solute volume fraction at $\Phi=10$. Comparison of the results of the $(3+1)$-parameter (continuum) solution with the *XYZ* solution is shown. Dotted lines show the single-phase values. Solid lines show phase coexistence. Note that there are two nematic phases in the *XYZ* solution.

VIII. CONCLUSIONS

In this paper we clarify the numerical difficulties encountered in solving a quantitative model of self-assembling spherocylinders, including the coupling between assembly and nematic order. The main quantity of interest is the equilibrium distribution of spherocylinder orientations and lengths. We begin with a transformation of the distribution and derive a nonlinear integral equation suitable for use as an iterative solution. Numerical iteration gives a monotonic decrease in the free energy and an incremental refinement of the distribution. In the isotropic phase the distribution converges rapidly. In the nematic phase the number of iterations required for convergence increases exponentially with increasing concentration, so an accurate distribution can only be found over a limited concentration range.

In the accessible range of nematic concentrations, we find that the distribution is *not* approximately Gaussian. Rather, it exhibits approximately linear behavior at small angles before reaching a plateau at a cutoff θ_1. The cutoff decreases exponentially with increasing volume fraction. This is the primary source of numerical difficulties since any discretization of the distribution must either resolve this cutoff or treat it in closed form. In calculations not presented here, we have verified that the linear regime and the smallness of θ_1 are not unique to the scaled particle expression for the effects of excluded volume [see Eq. (5)]. Onsager's second virial approximation [7] and the expression used by Hentschke and Herzfeld [19] yield qualitatively similar results. These observations provide a counterpoint to the common assumption that the nematic orientation distribution in self-assembling systems is Gaussian.

To extend the results to the full range of nematic concentrations, we introduce a trial distribution function that reproduces the qualitative features of the iterative solution. This allows us to solve most of the desired integrals in closed form and to treat some aspects of the solution analytically. The results of the trial function calculation suggest an approximate free energy for the nematic phase, valid for high volume fractions. From this we derive closed expressions for the free energy and the mean polymerization that are accurate to 1% for $v>0.7$ and seem to be *exact* in the limit $v\rightarrow 1$.

We find that the mean aggregation number in the nematic phase diverges at 100% solute volume fraction. (The divergence is above close packing due to our use of scaled particle theory.) As a result, the spherocylinder number density decreases to 0, as does the pressure. The only thermodynamically stable nematic phase has infinite mean polymerization and volume fraction $v=1$, indicating the formation of dense nematic crystallites in an otherwise isotropic solution. This agrees with the previous approximate results of Odijk [17] and van der Schoot and Cates [18], who conclude that the absence of a dilute nematic phase is due to the perfect rigidity of the rods. Flexibility will be relevant whenever the

mean filament length exceeds the persistence length. Approximate theories suggest that flexibility will smooth out the small-θ behavior of the orientation distribution and stabilize the nematic phase at lower volume fractions [17,29]. Another mitigating factor is the possibility of soft repulsions between the particles, which increase the relative cost of the dense phase and narrow the coexistence region [2].

The experimental systems that come closest in spirit to the present work are solutions of cylindrical micelles [6], sickle-cell hemoglobin [3,2], actin filaments [4], and microtubules [5]. All exhibit self-assembly and an isotropic-aligned phase transition as the solute concentration is increased. However, in all cases the width of the phase coexistence region is much narrower than predicted here. Actin filaments and surfactant micelles have significant electrostatic repulsion and are typically much longer than their persistence length. Microtubules and sickle cell hemoglobin filaments are less flexible, but soft repulsions are still believed to be relevant [30].

ACKNOWLEDGMENTS

This work was supported by NIH Grant No. HL36546 and NRSA Grant No. GM18932.

APPENDIX A: INTEGRALS S_1, $\langle\sigma\rangle$, AND Ψ

Substituting the trial function (39) into Eqs. (12) and (13) gives

$$s_1=\left[4\pi\int_0^{\pi/2}d\theta\,\sin(\theta)\frac{1}{1-g(\theta)}\right]^{-1}=\left[4\pi\left(\frac{1-\cos(\theta_1)}{1-g_0}+\frac{\theta_2-\theta_1}{\alpha}+\frac{\cos(\theta_2)}{1-g_2}\right)\right]^{-1}, \quad \text{(A1)}$$

$$\langle\sigma\rangle=4\pi s_1\left[\frac{1-\cos(\theta_1)}{(1-g_0)^2}+\frac{1}{\alpha^2}\ln\left(\frac{\tan(\theta_2/2)}{\tan(\theta_1/2)}\right)+\frac{\cos(\theta_2)}{(1-g_2)^2}\right]. \quad \text{(A2)}$$

The integral Ψ in Eq. (14) is

$$\Psi=4\pi s_1\left[\frac{g_0\ln(g_0)}{(1-g_0)^2}[1-\cos(\theta_1)]+\frac{I_A}{\alpha^2}+\frac{g_2\ln(g_2)}{(1-g_2)^2}\cos(\theta_2)\right], \quad \text{(A3)}$$

$$I_A=\int_{\theta_1}^{\theta_2}d\theta\,\frac{\ln[1-\alpha\,\sin(\theta)]}{\sin(\theta)}, \quad \text{(A4)}$$

where the integral I_A cannot be solved in terms of elementary functions. We calculate I_A by discretizing at N_θ points. Then

$$I_A=\Delta\theta\sum_{j=1}^{N_\theta}y_j\frac{\ln[1-\alpha\,\sin(\theta_j)]}{\sin(\theta_j)}, \quad \text{(A5)}$$

where $\theta_j=\theta_1+(j-1)\Delta\theta$, $\Delta\theta=(\theta_2-\theta_1)/(N_\theta-1)$, $y_1=y_{N_\theta}=1/2$, and $y_{j\neq1,N_\theta}=1$. We use $N_\theta=32$, for which Eq. (A5) may have an error of 1%. In practice I_A makes a relatively small contribution to $F_{\rm tot}$.

APPENDIX B: APPROXIMATION FOR W

We seek an approximation for the kernel W defined in Eq. (18):

$$W(\theta,\theta')=\frac{1}{2\pi}\int_0^{2\pi}d\phi|\sin(\gamma)|, \quad \text{(B1)}$$

$$\cos(\gamma)=\cos(\theta)\cos(\theta')+\sin(\theta)\sin(\theta')\cos(\phi). \quad \text{(B2)}$$

Begin with the Taylor series for $W(\theta,\theta')$ at small $\sin(\theta')$ in the domain $0\leqslant\theta'\leqslant\theta\leqslant\pi/2$. We use trigonometric identities to rewrite Eq. (B2):

$$\sin(\gamma)=\sin(\theta)\sqrt{1-\sin(\theta')\left(\frac{2\cos(\theta')\cos(\phi)}{\tan(\theta)}\right)+\sin^2(\theta')\left(\frac{1}{\tan^2(\theta)}-\cos^2(\phi)\right)}. \quad \text{(B3)}$$

Expanding the square root to second order in $\sin(\theta')$ and integrating over ϕ gives

$$W(\theta,\theta')=\sin(\theta)\left(1+c\frac{\sin^2(\theta')}{4\sin^2(\theta)}[1-2\sin^2(\theta)]\right), \quad \text{(B4)}$$

where $c=1$. This expression was compared to accurate data for W using MATHEMATICA. The relative error is only 2% at small θ', but this increases to 15% for θ' near $\pi/2$.

With the choice $c=1.3$, some accuracy is lost near the origin, but agreement is better than 7% over the whole domain. To illustrate the accuracy of the approximation, in the isotropic phase we find

$$\langle\sin(\gamma)\rangle=\frac{\pi}{2}-\frac{2}{3}-\frac{1.3}{10}=0.774\ldots, \quad \text{(B5)}$$

which is only 1.4% less than the exact value $\pi/4=0.785\ldots$.

APPENDIX C: INTEGRAL Γ

Substituting the approximate kernel $\tilde{W}$ into Eq. (17) gives

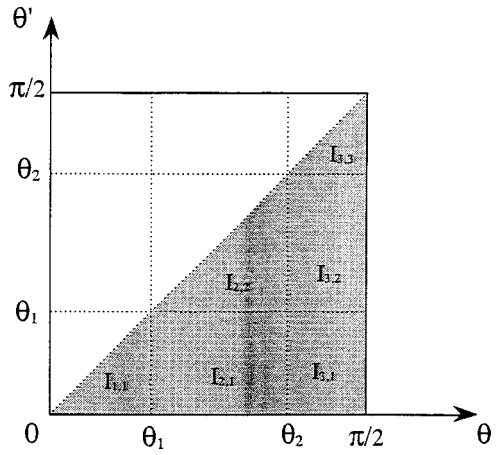

FIG. 12. Domains of integration used in the calculation of Γ.

$$\Gamma = 2a(4\pi s_1 \Delta l)^2 \int_0^{\pi/2} d\theta \frac{g(\theta)}{[1-g(\theta)]^2} \times \int_0^{\theta} d\theta' \frac{g(\theta')}{[1-g(\theta')]^2} \left\{ K_0(\theta,\theta') + \frac{c}{4} K_1(\theta,\theta') \right\}, \tag{C1}$$

where we have broken the kernel K into two pieces:

$$K_0(\theta,\theta') = \sin^2(\theta)\sin(\theta'), \tag{C2}$$

$$K_1(\theta,\theta') = \sin^3(\theta')[1-2\sin^2(\theta)]. \tag{C3}$$

K_0 is due to the zeroth-order term in the Taylor series of W [see Eq. (B4)] and K_1 is due to the second-order term. We have split the kernel in this way to clarify the integrations. Figure 12 shows the division of the integral for Γ into six domains

$$\Gamma = 2a(4\pi s_1 \Delta l)^2 \sum_{i=1}^{3} \sum_{j=1}^{i} \left\{ I_{i,j}^0 + \frac{c}{4} I_{i,j}^1 \right\}, \tag{C4}$$

$$I_{i,j}^k = \int_i d\theta\, h(\theta) \int_j d\theta' h(\theta') K_k(\theta,\theta'), \tag{C5}$$

where $h = g/(1-g)^2$. The integrals $I_{i,j}^k$ can all be solved in terms of elementary functions with the exception I_C indicated below:

$$I_{1,1}^j = h_0^2\, F_j(0,\theta_1), \tag{C6}$$

$$I_{3,3}^j = h_2^2\, F_j(\theta_2, \pi/2), \tag{C7}$$

$$F_0(\theta_1,\theta_2) = \left\{ \frac{1}{2}\cos(\theta_1)\left(\theta - \frac{\sin(2\theta)}{2} \right) - \frac{1}{3}\sin^3(\theta) \right\}_{\theta_1}^{\theta_2}, \tag{C8}$$

$$F_1(\theta_1,\theta_2) = \left\{ \frac{1}{6}\cos(\theta_1)[2+\sin^2(\theta_1)] - \frac{2}{3}\sin(\theta) + \frac{1}{3}\sin^3(\theta) + \frac{2}{15}\sin^5(\theta) \right\}_{\theta_1}^{\theta_2}, \tag{C9}$$

$$I_{2,1}^0 = h_0[1-\cos(\theta_1)]\left\{ \frac{1}{\alpha^2}\theta + \frac{1}{\alpha}\cos(\theta) \right\}_{\theta_1}^{\theta_2}, \tag{C10}$$

$$I_{2,1}^1 = -h_0 c_1 \left\{ \frac{1}{\alpha^2 \tan(\theta)} + \frac{2}{\alpha^2}\theta + \frac{1}{\alpha}\ln[\tan(\theta/2)] + \frac{2}{\alpha}\cos(\theta) \right\}_{\theta_1}^{\theta_2}, \tag{C11}$$

$$c_1 = \frac{2}{3}[1-\cos(\theta_1)] - \frac{1}{3}\cos(\theta_1)\sin^2(\theta_1), \tag{C12}$$

$$I_{3,1}^0 = h_0 h_2 \frac{1}{2}[1-\cos(\theta_1)]\left(\frac{\pi}{2} - \theta_2 + \frac{\sin(2\theta_2)}{2} \right), \tag{C13}$$

$$I_{3,1}^1 = -\frac{1}{2} h_0 h_2 c_1 \sin(2\theta_2), \tag{C14}$$

$$I_{3,2}^0 = \frac{h_2}{2}\left(\frac{\pi}{2} - \theta_2 + \frac{\sin(2\theta_2)}{2} \right)\left\{ \frac{1}{\alpha^2}\ln(\theta/2) - \frac{\theta}{\alpha} \right\}_{\theta_1}^{\theta_2}, \tag{C15}$$

$$I_{3,2}^1 = \frac{h_2}{2}\sin(2\theta_2)\left\{ \frac{1}{\alpha^2}\cos(\theta) + \frac{1}{2\alpha}\left(\theta - \frac{\sin(2\theta)}{2} \right) \right\}_{\theta_1}^{\theta_2}, \tag{C16}$$

where $h_0 = g_0/(1-g_0)^2$, $h_2 = g_2/(1-g_2)^2$, and $\{A(\theta)\}_{\theta_1}^{\theta_2} = A(\theta_2) - A(\theta_1)$.

The integration $I_{2,2}$ involves four pieces. Rewriting h for $\theta_1 \leqslant \theta \leqslant \theta_2$,

$$h = \frac{1}{[\alpha\,\sin(\theta)]^2} - \frac{1}{\alpha\,\sin(\theta)}, \tag{C17}$$

gives

$$I_{2,2}^j = \frac{1}{\alpha^4} I_{s^2 s^2}^j - \frac{1}{\alpha^3} I_{s^2 s}^j - \frac{1}{\alpha^3} I_{ss^2}^j + \frac{1}{\alpha^2} I_{ss}^j, \tag{C18}$$

$$I_{s^\kappa s^\lambda}^j = \int_{\theta_1}^{\theta_2} d\theta\, \frac{1}{\sin^\kappa(\theta)} \int_{\theta_1}^{\theta} d\theta'\, \frac{1}{\sin^\lambda(\theta')} K_j(\theta,\theta'), \tag{C19}$$

$$I_{ss}^0 = \{\sin(\theta) - \cos(\theta_2)\theta\}_{\theta_1}^{\theta_2}, \tag{C20}$$

$$I_{s^2 s}^0 = \frac{1}{2}(\theta_2 - \theta_1)^2, \tag{C21}$$

$$I_{ss^2}^0 = \{-\cos(\theta_2)\ln[\tan(\theta/2)] + \ln[\sin(\theta)]\}_{\theta_1}^{\theta_2}, \tag{C22}$$

$$I_{s^2 s^2}^0 = \{\theta_2 \ln[\tan(\theta/2)]\}_{\theta_1}^{\theta_2} - I_C, \tag{C23}$$

$$I_C = \int_{\theta_1}^{\theta_2} d\theta \frac{\theta}{\sin(\theta)} = \Delta\theta \sum_{j=1}^{N_\theta} y_j \frac{\theta_j}{\sin(\theta_j)}, \tag{C24}$$

where I_C is the second integral that must be calculated numerically [see Eq. (A5) for notation]. The remaining integrals are

$$I^1_{ss}=\left\{-\left(\theta_1-\frac{\sin(2\theta_1)}{2}\right)\left(\frac{1}{2}\ln[\tan(\theta/2)]+\cos(\theta)\right)-\frac{3}{2}\sin(\theta)+\frac{1}{3}\sin^3(\theta)+\theta\cos(\theta)\right\}_{\theta_1}^{\theta_2}+\frac{1}{2}I_C, \tag{C25}$$

$$I^1_{s^2s}=\frac{1}{2}\left\{\left(\theta_1-\frac{\sin(2\theta_1)}{2}\right)\left(\frac{1}{\tan(\theta)}+2\theta\right)-\frac{\theta}{\tan(\theta)}+\sin^2(\theta)-\theta^2\right\}_{\theta_1}^{\theta_2}, \tag{C26}$$

$$I^1_{s^2s^2}=\left\{-\cos(\theta_1)\left(\frac{1}{\tan(\theta)}+2\theta\right)+\frac{1}{\sin(\theta)}+2\sin(\theta)\right\}_{\theta_1}^{\theta_2}, \tag{C27}$$

$$I^1_{ss^2}=\{\cos(\theta)\ln[\tan(\theta/2)]-\ln[\sin(\theta)]+\sin^2(\theta)+2\cos(\theta_1)\cos(\theta)\}_{\theta_1}^{\theta_2}. \tag{C28}$$

APPENDIX D: SINGULAR BRANCH IN THE P-μ PLANE

Consider a Helmholtz free energy of the form $F_{\rm tot}[T,V,M,s_\sigma(\Omega)]=F_{\rm ns}+F_s$, where $F_{\rm ns}$ contains all nonsingular terms and F_s diverges at v_s and is only appreciably different from zero in the infinitesimal neighborhood $v_s-\epsilon\leqslant v\leqslant v_s$. [In Sec. VI C, $v_s=1$ and $\epsilon\sim(a/L)^{1/3}\ll 1$.] Since the free energy is an extensive quantity, we can write $F_s[T,V,M,s_\sigma(\Omega)]=Vf[T,v,s_\sigma(\Omega)]$, where $v=MV_1/V$ is the volume fraction. The pressure and chemical potential are

$$p(v)=-\frac{\partial F_{\rm tot}}{\partial V}=p_{\rm ns}(v)-f+vf', \tag{D1}$$

$$\mu(v)=\frac{\partial F_{\rm tot}}{\partial M}=\mu_{\rm ns}(v)+V_1f', \tag{D2}$$

where $f'=\partial f/\partial v$ and the subscript ns denotes the nonsingular contributions. We only need to show that $f\ll vf'$. Recalling that F_s is negligible for $v\leqslant v_s-\epsilon$ and assuming that f' is montonically increasing, we find the bound

$$f(v)=\int_{v_s-\epsilon}^{v}dv'f'(v')\leqslant f'(v)(v-v_s+\epsilon). \tag{D3}$$

In the domain $v_s-\epsilon\leqslant v\leqslant v_s$ this implies

$$f'(v)\geqslant\frac{f(v)}{v-v_s+\epsilon}\gg f(v), \tag{D4}$$

where we have used the fact that $\epsilon\ll 1$. Equations (D1) and (D2) thus give

$$\mu-\mu_{\rm ns}(v_s)=\frac{V_1}{v_s}[p-p_{\rm ns}(v_s)]. \tag{D5}$$

In Sec. V C, $v_s=1$ and $p_{\rm ns}(v_s)=\mu_{\rm ns}(v_s)=0$, giving $\mu=V_1p$, the desired result.

[1] J. Herzfeld, Acc. Chem. Res. **29**, 31 (1996).
[2] W. A. Eaton and J. Hofrichter, Adv. Protein Chem. **40**, 63 (1990).
[3] M. S. Prouty, A. N. Schechter, and V. A. Parsegian, J. Mol. Biol. **184**, 517 (1985).
[4] A. Suzuki, T. Maeda, and T. Ito, Biophys. J. **59**, 25 (1991).
[5] A. Hitt, A. Cross, and R. Williams, J. Biol. Chem. **265**, 1639 (1990).
[6] M. P. Taylor and J. Herzfeld, J. Phys.: Condens. Matter **5**, 2651 (1993), and references therein.
[7] L. Onsager, Ann. (N.Y.) Acad. Sci. **51**, 627 (1949).
[8] M. A. Cotter and D. C. Wacker, Phys. Rev. A **18**, 2669 (1978).
[9] A. Stroobants, H. N. W. Lekkerkerker, and T. Odijk, Macromolecules **19**, 2232 (1986).
[10] A. R. Khokhlov and A. N. Semenov, Physica A **108**, 546 (1981); **112**, 605 (1982).
[11] T. Odijk, Macromolecules **19**, 2313 (1986).
[12] G. J. Vroege and H. N. W. Lekkerkerker, Rep. Prog. Phys. **55**, 1241 (1992).
[13] W. E. McMullen, W. M. Gelbart, and A. Ben-Shaul, J. Chem. Phys. **82**, 5616 (1985).
[14] R. Hentschke and J. Herzfeld, Phys. Rev. A **43**, 7019 (1991).
[15] T. L. Madden and J. Herzfeld, Biophys. J. **65**, 1147 (1993).
[16] J. Herzfeld and R. Briehl, Macromolecules **14**, 397 (1981).
[17] T. Odijk, J. Phys. (Paris) **48**, 125 (1987).
[18] P. van der Schoot and M. Cates, Langmuir **10**, 670 (1994).
[19] R. Hentschke and J. Herzfeld, J. Chem. Phys. **90**, 5094 (1989).
[20] There is some debate in the literature about the correct form for the translational contribution. See Refs. [13] and [18].
[21] P. Mukerjee, J. Phys. Chem. **76**, 565 (1972).
[22] H. Reiss, H. L. Frisch, and J. L. Lebowitz, J. Chem. Phys. **31**, 369 (1959).
[23] P. Bolhuis and D. Frenkel, J. Chem. Phys. **106**, 666 (1997).
[24] W. H. Press *et al.*, *Numerical Recipes* (Cambridge University Press, New York, 1989).
[25] R. W. Briehl and J. Herzfeld, Proc. Natl. Acad. Sci. USA **76**, 2740 (1979).
[26] M. Cotter and D. Martire, J. Chem. Phys. **53**, 4500 (1970).
[27] R. Zwanzig, J. Chem. Phys. **39**, 1714 (1963).
[28] J. Herzfeld and M. P. Taylor, J. Chem. Phys. **88**, 2780 (1988).
[29] R. Hentschke, Liq. Cryst. **10**, 691 (1991).
[30] J. Han and J. Herzfeld, Biopolymers **45**, 299 (1998).